Optical and Quantum Electronics (2023) 55:1241
https://doi.org/10.1007/s11082-023-05560-8

Research on wideband dissipative soliton generation and the dynamics process

Yong Zhou[1] · Yangyang Wang[1] · Xian Wang[1] · Kai Zhang[1] · Xiaohui Ma[1] · Wentan Fang[1] · Xiaolin Chen[1] · Wei Zhang[1] · Song Huang[1] · Weiqing Gao[1]

Received: 18 August 2023 / Accepted: 7 October 2023 / Published online: 25 October 2023

Abstract
Wideband dissipative soliton is generated in a passively mode-locked cavity by optimizing the distribution of chromatic dispersion and gain filtering in cavity. The maximal 3 dB bandwidth of 61.1 nm is obtained. The corresponding pulse width is compressed to 222 fs with chirp, which could be further compressed to 42 fs according to the Fourier transform limitation. The signal-to-noise ratio is 80.3 dB. The single pulse energy is 0.18 nJ. The dynamics process is investigated by dispersive Fourier transformation during the building-up. The simulation investigation on dissipative soliton formation is provided according to the modified nonlinear Schrödinger equation, which are relatively consistent with the experiment. The results demonstrate that a weak normal net dispersion close to zero and efficient gain bandwidth are critical to the formation of wideband dissipative soliton.

Keywords Dispersive Fourier transformation · Mode-locked fiber lasers · Wideband dissipative soliton · Nonlinear Schrödinger equation

1 Introduction

Passively mode-locked fiber laser is widely used in laser machining, frequency comb generation, and nonlinear optics due to the ultra-short pulse duration and high peak power. Ultrafast fiber laser as an important branch in laser field has been developed as an important platform for soliton dynamics. Corresponding to the experiment, recent researches had obtained systematically theoretical study on soliton dynamics (Liu et al. 2022; Yan and Liu 2022; Wang et al. 2022, 2022a, 2023). Dissipative solitons (DSs) arise from a balance among self-phase modulation (SPM) effect, dispersion, and gain/loss (Grelu and Akhmediev 2012). DSs in dissipative fiber laser systems operating in the normal dispersion regime exhibit extremely complex and interesting dynamics. Compared with conventional solitons (CSs) and dispersion-managed solitons, DSs can withstand more nonlinear phase shifts to avoid soliton splitting (Cui et al. 2016). This property is benefit for high power amplification, which have attracted extensive researches. Wideband solitons can be used as the light

Extended author information available on the last page of the article

source in optical coherence tomography (OCT) (Wang et al. 2019a) systems for biomedical imaging. In 2021, broadband dispersion-managed soliton obtained in mode-locked fiber laser is incorporated into the swept source OCT system. High resolution and imaging speed was achieved by time stretching (Chen et al. 2021). In addition, the wideband dissipative solitons provide an excellent approach for highly coherent light sources (Gao et al. 2019), frequency comb (Picqué and Hänsch 2019), and so on. The study of wideband DS is of great significance due to the potential applications.

According to previous reports, the spectral bandwidth of DS is closely related to dispersion distribution, net dispersion and intracavity gain/loss. Kang (Kang et al. 2018) reported a dissipative soliton with 10 dB bandwidth of 52.4 nm. The 3 dB bandwidth of dissipative solitons output by Wang et al. (2019) in similar cavities is 47.8 nm, which proves that spectral filtering and appropriate linear cavity loss are the key to the formation of L-band DSs. The 2D materials has the advantages of fast relaxation and high modulation depth, which are benefit for the ultra-fast pulse generation. Some previous works had demonstrated the dissipative soliton generation with 2D materials (Xu et al. 2020; Chai et al. 2018; Li et al. 2021), but the integration method may cause high insertion loss and realized in the problem of higher pump power and low lifetime. However, no report has systematically studied the key factors in the formation of broadband dissipative solitons. In recent years, the development of Dispersive Fourier transformation (DFT) technology for real-time measurement of ultrafast laser spectra has also driven the trend of soliton dynamics research (Goda et al. 2013; Wang et al. 2020). Due to the characteristics of comprehensive equilibrium, DS has more unusual and interesting dynamics than CS, such as soliton explosion (Liu et al. 2020; Zhou et al. 2020a), soliton molecules (Zhou et al. 2020b; Zhou et al. 2022), pulse solitons (Zheng et al. 2021; Du et al. 2021) and so on.

In this letter, we realized a DS mode-locked fiber laser (DS-MLFL) by NPR with wide spectrum covering C+L band. Wideband DSs with 3 dB bandwidth of 61.1 nm were obtained. The pulse width was compressed to 222 fs after amplification. The real-time spectral evolution during the build-up process of DS generation was observed by DFT technique. According to the modified nonlinear Schrödinger equation (NLSE), we simulated and analyzed the effect of intracavity dispersion distribution and gain filtering on the spectral bandwidth, which helps to optimize the broadband dissipative soliton laser. The results show that both weak normal net dispersion close to zero and sufficient gain bandwidth are the necessary for wideband DS generation, which are relatively consistent with the experiment. The research results can provide effective guidance for the subsequent generation of wideband DS.

2 Experimental setup

The experimental setup of wideband DS fiber laser is shown in Fig. 1. The cavity consists of three types of optical fibers, including 0.34 m HI1060 fiber (Corning, β_2 = -10 ps²/km @1550 nm), 12.6 m erbium-doped fiber (EDF, Fibercore I4, β_2=+6.98 ps²/km @1550 nm), and 3.34 m single-mode fiber (SMF, Corning SMF-28e, β_2 = -22 ps²/km @1550 nm). The total cavity length is 16.28 m. HI1060 fiber appears in the structure as the pigtail of 980/1550 nm wavelength division multiplexer (WDM). The net dispersion of cavity is ~0.011 ps². The length of EDF was set as 12.6 m to obtain the amplified spontaneous emission (ASE)

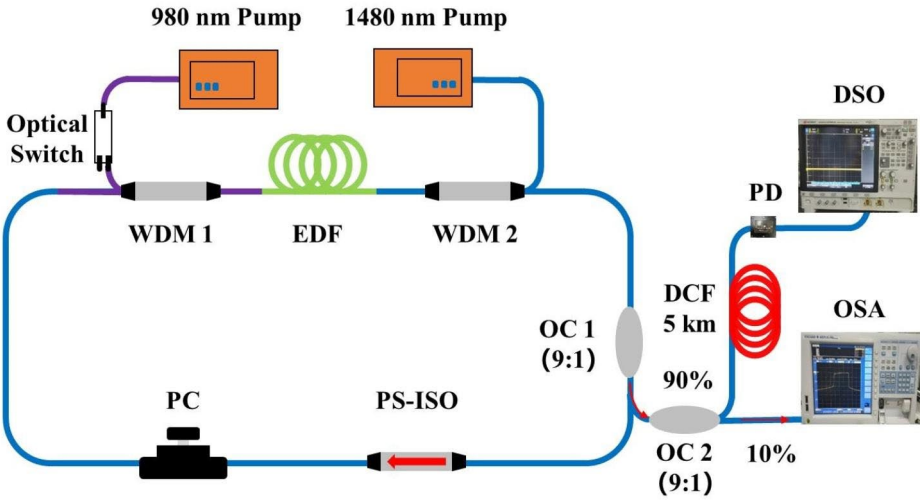

Fig. 1 Scheme of the wideband DS fiber laser and measurement setup

spectrum covering C+L band, which reflected the cavity gain profile. The length of SMF was adjusted to realize the weak normal net dispersion.

We used 980 nm, 1480 nm wavelengths of laser diodes (LDs) pumped in both directions to increase the gain bandwidth covering the C+L band. Since there may be residual pumping under strong pump, the pump LDs with two different wavelengths were used to prevent the LD damage. The optical switch was used to provide fast pump modulation with a response time of less than 1 μs. The fast pump modulation could reduce the start time of mode-locking state effectively. The DS was generated by NPR through the polarization controller (PC) and polarization sensitive isolator (PS-ISO) in the cavity. NPR worked as a saturable absorber (SA) in the cavity, providing mode-locking mechanism and large modulation depth. PS-ISO ensured the unidirectional propagation of signal light in the cavity, and compressed the operating pulse. The operating pulses output through the 10% port of optical coupler (OC1). The small coupling ratio was chosen to reduce the cavity loss and make it easier to start the mode-locking. The emitted pulses were divided into two branches through OC2. The large branch from the 90% port was connected to the photodetector (PD, Optilab, PD-23-C-AC, bandwidth 23 GHz) to measure the temporal properties. The pulse train was measured with the real-time digital storage oscilloscope (DSO, RIGOL MSO8000) with a sampling rate of 10 GSa/s. The radio frequency (RF) spectrum of the output pulse was recorded by RF spectrum analyzer (Keysight N9000B, bandwidth 26 GHz). The small branch from the 10% port was connected to the optical spectrum analyzer (OSA, Yokokawa AQ6375) with the highest resolution of 0.05 nm. The autocorrelation trace (AC) of the pulse was measured by an autocorrelator (APE, pulseCheck 150). In order to record the real-time spectrum after stretched by large dispersion medium, the pulses from the 90% port of OC2 were launched into 5 km long dispersion compensating fiber (DCF, YOFC G652.C DM1010-D, β_2=+172 ps^2/km). The spectrum of each pulse was mapped into temporal domain and recorded by the DSO.

3 Experimental results

When the pump power of the 976 nm and the 1480 nm LDs were set as 57 mW and 14 mW, respectively. The stable mode-locking was obtained at suitable polarization state. Since the peak power of this laser is weaker than that of common conventional soliton, the pulse need stronger pump to realize mode-locking by nonlinear polarization rotation. In addition, the signal in L band is more difficult to obtain gain from EDF, which means the pulse operated in L band need stronger pump than that in C band. As a result, the mode-locked threshold may not be further decreased to the level of common conventional solitons. The average power was 2.2 mW, the energy power could be improved by the further amplifier. Figure 2(a) shows the average spectrum measured by the OSA, which has typical rectangular type of DS. The central wavelength is 1561.1 nm and the 3 dB bandwidth is 61.1 nm. The corresponding Fourier transform limitation is 42 fs. Due to the bidirectional pumping, the gain profile is more evenly distributed in the gain fiber, which can effectively increase the gain bandwidth and be benefit to improve gain spectrum range (Wang et al. 2016; Wang et al. 2016a; Ahmad et al. 2014). The pulse period is 81.5 ns, as shown in Fig. 2(b). The single pulse energy is 0.18 nJ, which is limited by the long cavity length to avoid soliton splitting. According to the RF spectrum in Fig. 2(c) measured with the resolution of 100 Hz, the fundamental frequency is 12.27 MHz with the signal-to-noise ratio (SNR) of 80.3 dB. The high SNR is a strong evidence of the good stability of mode-locking. The harmonic frequencies in the range of 1 GHz are presented as the inset in Fig. 2(c), which shows good flatness and

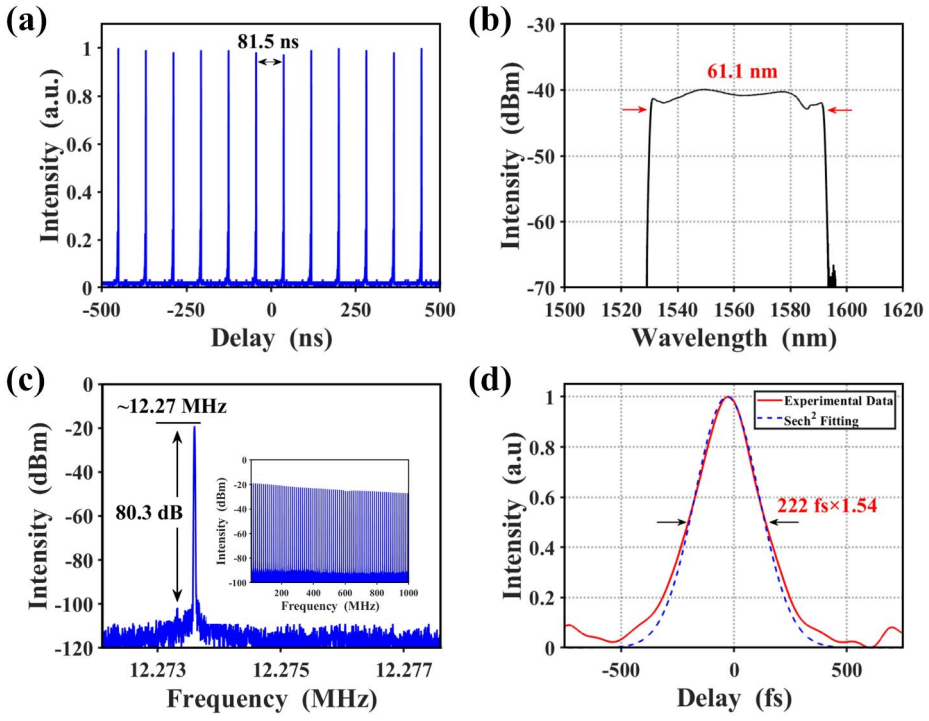

Fig. 2 Properties of the mode-locking pulses. (**a**) Optical spectrum in logarithmic scale; (**b**) pulse train; (**c**) RF spectrum (inset: harmonics frequencies within 1 GHz); (**d**) autocorrelation trace

low pedestal. As the peak power was too low to measure the autocorrelation trace directly, the emitted pulses were amplified with a homemade erbium-doped fiber amplifier. The trace width is 342 fs as shown in Fig. 2(d), corresponding to the pulse duration of 222 fs by $sech^2$ fitting. Because the emitted pulses were compressed by SMF, $sech^2$ fitting was used. The time-bandwidth product is 1.67, indicating that the pulse width can be further compressed. The strong SPM in amplifier fibers would introduce additional positive chirp and made the time-bandwidth product exceed the Fourier transform limitation. After amplification, the solitons were easy to split in the SMF due to the SPM caused by high peak power. Therefore, the appropriate SMF length is selected to compress the pulse width to the maximum extent.

Figure 3(a) shows the build-up process of DSs measured by DFT technique cooperating with PD and DSO. The compared spectra measured by OSA and DFT technique in linear scale is shown in Fig. 3(b). The real-time spectrum obtained by DFT technique shows the same shape with the averaged spectrum by OSA. As the small pulses jittered with time are absorbed, main pulse with central wavelength of 1561 nm is amplified before the 800th roundtrip, and then the spectrum is broadened rapidly from the 800th to 850th roundtrip. About 340 roundtrips from the 850th to 1190th represent the critical mode-locking state, according to the zoomed figure as shown in Fig. 3(c). Finally, the stable mode-locking state was formed after the 1190th roundtrip. Figure 3(d)-3(e) represent the typical spectra of unstable states with obvious power vibration.

4 Simulation

To investigate the main factors affecting the spectral bandwidth in the process of DS pulse generation including gain filtering effect, net dispersion and dispersion distribution, we numerically simulated the laser operation based on the modified NLSE, as described in

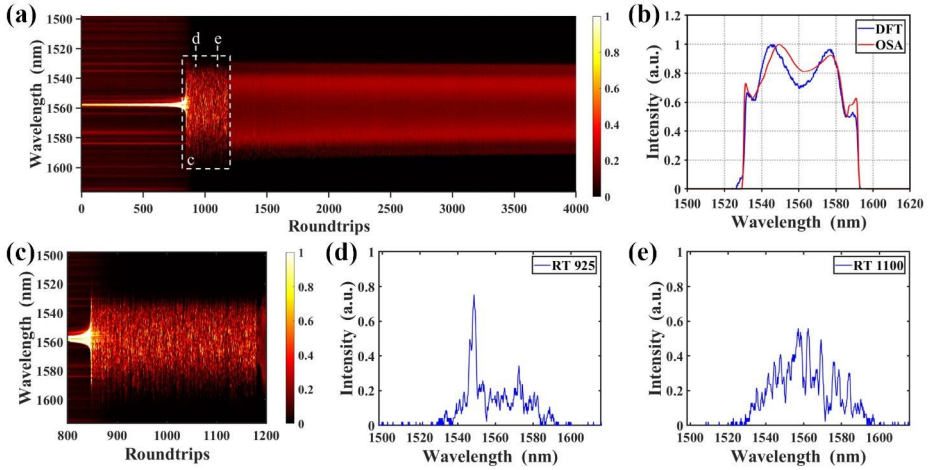

Fig. 3 Build-up dynamics of the DSs. (**a**) Spectral evolution of each roundtrip; (**b**) spectra in linear scale measured by OSA (red line) and DFT technique (blue line); (**c**) zooming in of the critical mode-locking part; (**d-e**) single shots of the 925th and 1100th roundtrips, respectively

Refs. (Wang et al. 2020; Song et al. 2019). The pulse propagation in optical fiber is modeled by the modified NLSE:

$$\frac{\partial U}{\partial z} = -\frac{i\beta_2}{2}\frac{\partial^2 U}{\partial t^2} + i\gamma|U|^2 U + \frac{g-\alpha}{2} + \frac{g}{2}\frac{1}{\Omega_g^2}\frac{\partial^2 U}{\partial t^2} \tag{1}$$

where, U is the slowly varying envelope, z is the propagation distance, β_2 is the GVD parameter, γ is the nonlinear parameter, Ωg is the gain bandwidth and α represents the loss coefficient. The laser gain g is defined as $g=g_0\exp(-E_{ave}/E_{sat})$ for EDF, where $g_0=0.06\ \mathrm{m}^{-1}$ is the small signal gain (Lyu et al. 2017), E_{ave} is the average pulse energy (the integration of the instantaneous power P_{in} within calculation window) and the saturated energy of E_{sat} = 118 pJ depends on the pump power (Zhao et al. 2021). The nonlinear coefficient, dispersion coefficient and length of the three fibers used in simulation are shown in Table I. The nonlinear transmittance affecting the saturable effect is determined by $T=\exp[-\Delta t/(1+P_{in}/P_{sat})]$, where $\Delta t=0.6$ corresponds to the modulation depth, and $P_{sat}=55$ W is the saturation power. In order to verify the rationality of the simulation process, the simulated laser structure was consistent with the experiment. The output ratio is 10%.

In the simulation, we investigated the gain filtering affected by changing the gain bandwidth Ωg from 30 to 80 nm, as shown in Fig. 4(a). The corresponding DFT evolution is shown as in Fig. 4(c). The results show that when the gain bandwidth is narrow, the operating pulse cannot be effectively amplified, resulting in unstable mode-locking states until the gain and nonlinear transmittance is adjusted.

When the gain bandwidth reached 53 nm, stable DS operation with 3 dB bandwidth of 65.1 nm was obtained. The spectral width remains unchanged with the gain bandwidth increasing. In this situation, the spectral width is mainly limited by the intra-cavity dispersion distribution. To investigate the influence of net dispersion on the spectral width, the net dispersion was varied from -37.8×10^{-3} ps^2 to $+49.12\times10^{-3}$ ps^2, the Ωg is fixed at 55 nm. When the net dispersion is negative, strong SPM effect is induced by the short duration in the long fiber and results in chaotic pulse splitting, as shown in Fig. 4(b, d). The typically split pulse revolution is shown in the insets on Fig. 4(a, b). The output spectrum shows strong and unstable interaction between the split pulses. Under the above conditions, the calculated spectral bandwidth changes disorderly. Additionally, the bandwidth of CS in negative dispersion cavity is narrower than DS, so the details are not discussed here. When the net dispersion is near 5×10^{-3} ps^2, the spectral bandwidth increases rapidly to the maximum of 65.1 nm. As the net dispersion continues to increase, the spectral bandwidth descends to a stable value.

To investigate the influence of intra-cavity dispersion distribution, we observed the pulse operation details with the net dispersion of 5×10^{-3} ps^2. The spectral width is 65.1 nm as shown in Fig. 5(a) with a flat top. The spectral evolution of the soliton build-up process is shown in Fig. 5(b), which agrees well with the experimental results as in Fig. 3(a). However, the gain characteristic evolution of EDF caused by the relaxation oscillation was not

Table 1 Parameters Used in the Simulations

Parameters	EDF	SMF	HI1060
γ (W^{-1} m^{-1})	6.5×10^{-3}	1.5×10^{-3}	1.5×10^{-3}
α (dB m^{-1})	3.5×10^{-3}	0.3×10^{-3}	0.3×10^{-3}
β_2 (ps^2/km)	6.5	-22	-10
L (m)	12.6	3.34	0.34

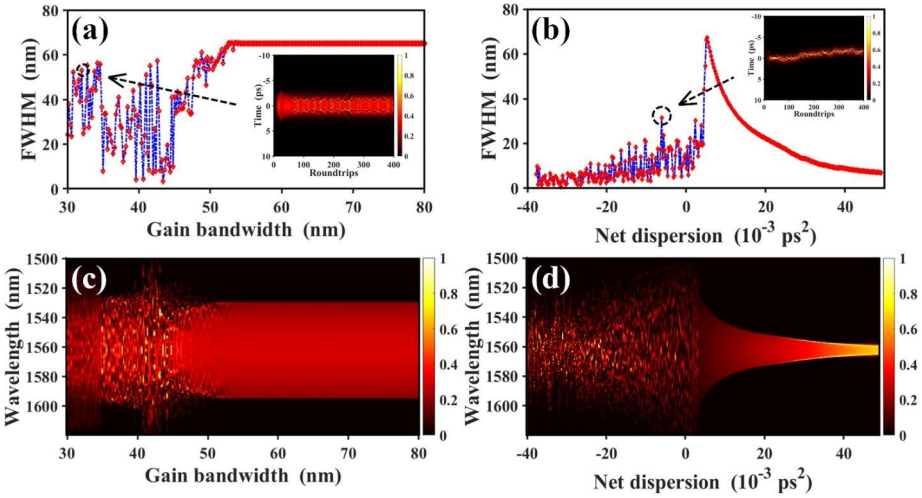

Fig. 4 Simulation results: spectral width and output spectrum varied with (**a, c**) gain bandwidth and (**b, d**) net dispersion. Insets: The pulse evolution characteristics at gain bandwidth of 32 nm and net dispersion of -6.18×10^{-3} ps^2

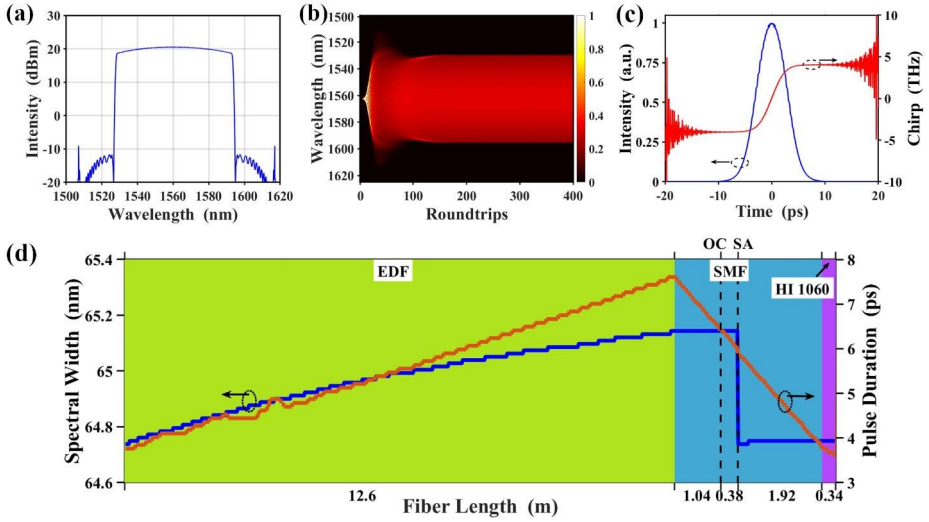

Fig. 5 Simulated properties of the wideband DS. (**a**) Corresponding spectrum with 3 dB bandwidth of 65.1 nm; (**b**) spectral evolution; (**c**) soliton pulse with chirp characteristics; (**d**) pulse parameters operation in cavity (blue line: spectral width; orange line: pulse duration)

considered, so the simulation results could not show the unstable states as in the experiment. The intensity distribution of temporal domain and the chirp characteristics is shown in Fig. 5(c), where the pulse shows a typical linear positive chirp across the DSs. Figure 5(d) shows the evolvement of spectral bandwidth and pulse duration in the cavity. In EDF with normal dispersion, the pulse obtains positive chirp, and the spectral bandwidth is broadened

synchronously with pulse duration. In the SMF and HI1060 with anomalous dispersion, the spectral width shows no obvious change except for the slightly narrowing by the SA. According to the numerical results, there is minimal spectral broadening in anomalous dispersion fiber caused by SPM, but it cannot be recognized in Fig. 5(d) because of the plotting resolution. The pulse duration is consecutively compressed at SMF, SA and HI1060, reaches the minimum value, and returns to the same value before EDF to complete self-consistency. From the trend of pulse duration, it is noticed that there is only one minimum pulse duration in cavity, which is different from the periodic pulse broadening and compression in stretched pulse laser which have two minimum values (Kang et al. 2018; Wang et al. 2013). According to the simulation results in Fig. 5(d), the spectral width is not sensitive to the output position.

Therefore, we can draw the conclusion from Fig. (4) that sufficient gain bandwidth and weak normal net dispersion are dominant to the formation of wideband DSs. Hence, the cavity gain profile need to be clarified of more than 50 nm before the laser design. Furtherly, the anomalous dispersion fiber length should be adjusted to meet the weak normal net dispersion with given EDF length. From Fig. 5, the spectral width varies less with the position inside cavity under this setup, which means the output position has minor impact on the spectral width.

5 Conclusion

In conclusion, we reported a wideband DS-MLFL with the central wavelength of 1561.1 nm and the 3 dB bandwidth of 61.1 nm by bidirectional pump. The pulse width was compressed to 222 fs after amplification. The spectral evolution during the build-up process was investigated experimentally by the DFT technique. Through the numerical simulation considering gain bandwidth, net dispersion and pulse evolution in cavity, the physical mechanism of the formation of wideband DSs was explored. It was found that sufficient gain bandwidth and weak normal net dispersion are the key factors for the formation of wideband DSs. The obtained wideband DSs have potential applications in optical communication, sensing and medical diagnosis.

Author contributions Yong Zhou, Yangyang Wang, Xian Wang and Song Huang contributed to the experiment and paper writing, Kai Zhang, Xiaohui Ma and Wentan Fang contributed to the data processing, Xiaolin Chen and Wei Zhang contributed to the simulation coding, Weiqing Gao contributed to the research idea and paper revision. All authors reviewed the manuscript.

Funding This work was supported by the National Natural Science Foundation of China under Grants 51972317, 61875052, 62105087, 62105088 and 61905059, the Anhui Provincial Key Research and Development Plan Grant 202104a07020010.

Data Availability The datasets used or analyzed during the current study are available from the corresponding author on reasonable request.

Declarations

Competing interests The authors declare no competing interests.

Conflict of interest The authors declare no conflicts of interest.

Ethical approval The contents of this manuscript have not been copyrighted or published previously; The contents of this manuscript are not now under consideration for publication elsewhere.

References

Ahmad, H., Zulkifli, A., Muhammad, F., Zulkifli, M., Thambiratnam, K., Harun, S.: Mode-locked L-band bismuth–erbium fiber laser using carbon nanotubes. Appl. Phys. B. **115**, 407–412 (2014)

Chai, T., Li, X., Feng, T., Guo, P., Song, Y., Chen, Y., Zhang, H.: Few-layer bismuthene for ultrashort pulse generation in a dissipative system based on an evanescent field. Nanoscale. **37**, 10 (2018)

Chen, H., Li, Y., Huang, D., Li, F., Lu, C., Wai: P.:114 nm broadband all-fiber nonlinear polarization rotation mode locked-laser and time-stretch optical coherence tomography. Opt. Express. **29**, 33322–33330 (2021)

Cui, Y., Lu, F., Liu, X.: MoS2-clad microfibre laser delivering conventional, dispersion-managed and dissipative solitons. Sci. Rep. **6**, 30524 (2016)

Du, W., LI, H., Li, J., Wang, Z., Zhang, Z., Zhang, S., Liu: Yong.: Real-time observation of pulsating period-doubled vector solitons in a passively mode-locked fiber laser. Optics Express, 29, 14101–14111, (2021)

Gao, L., Cao, Y., Wabnitz, S., Ran, H., Kong, L., Li, Y., Huang, W., Huang, L., Feng, D., Zhu: Tao.: Polarization evolution dynamics of dissipative soliton fiber lasers. Photon. Res. 7, 1331–1339 (2019)

Goda, K., Jalali, B.: Dispersive Fourier transformation for fast continuous single-shot measurements. Nat. Photonics. **7**, 102–112 (2013)

Grelu, P., Akhmediev, N.: Dissipative solitons for mode-locked lasers. Nat. Photonics. **6**, 84–92 (2012)

Kang, J., Kong, C., Feng, P., Wei, X., Luo, Z., Edmund, Y., Kenneth, K.: Broadband High-Energy All-Fiber laser at 1.6 μm. IEEE Photonics Technol. Lett. **30**, 311–314 (2018)

Lyu, Y., Zou, X., Shi, H., Liu, C., Wei C., Li J., Li H., Liu Y.: Multipulse dynamics under dissipative soliton resonance conditions. Opt. Express. **25**, 13286–13295 (2017)

Li, L., Pang, L., Wang, R., Zhang, X., Hui, Z., Han, D., Zhao, F., Liu, W.: Ternary transition metal dichalcogenides for high power vector dissipative soliton ultrafast fiber laser. Laser Photonics Rev. **16**, 2 (2021)

Liu, M., Li, T., Luo, A., Xu, W., Luo, Z.: Periodic soliton Explosions in a dual-wavelength mode-locked Yb-doped fiber laser. Photonics Res. **8**, 246–251 (2020)

Liu, X., Zhang, H., Liu, W.: The dynamic characteristics of pure-quartic solitons and soliton molecules. Appl. Math. Model. **102**, 305–312 (2022)

Picqué, N., Hänsch, T.: Frequency comb spectroscopy. Nat. Photonics. **13**, 146–157 (2019)

Song, Y., Shi, X., Wu, C., Tang, D., Zhang, H.: Recent progress of study on optical solitons in fiber lasers. Appl. Phys. Reviews. **6**, 21313 (2019)

Wang, Z., Wang, Y.: Sub-100 fs and Passive Harmonic Mode-Locking of Dispersion-Managed Dissipative Fiber Laser with Carbon nanotubes. J. Lightwave Technol. **31**, 3719–3725 (2013)

Wang, Z., Zhan, L., Fang, X., Gao, C., Qian, K.: Generation of Sub-60 fs Similaritons at 1.6 μm from an All-Fiber Er-Doped laser. J. Lightwave Technol. **34**, 4128–4134 (2016)

Wang, Z., Qian, K., Fang, X., Gao, C., Luo, H., Zhan, L.: Sub-90 fs dissipative-soliton Erbium-d oped fiber lasers operating at 1.6 μm band. Opt. Express. **24**, 10841–10846 (2016a)

Wang, X., Liu, Y., Wang, Z., Yang, G.: L-Band efficient dissipative Soliton Erbium-Doped Fiber laser with a Pulse Energy of 6.15 nJ and 3 dB bandwidth of 47.8 nm. J. Lightwave Technol. **37**, 1168–1173 (2019)

Wang, J., Tao, K., Zhu, W., Jiang, J., Liu, T.: A FBG-OCT catheter to reconstruct vascular shape in Intravascular Optical Coherence Tomography. IEEE Photonics Technol. Lett. **31**, 701–704 (2019a)

Wang, Y., Wang, C., Zhang, F., Guo, J., Ma, C., Huang, W., Song, Y., Ge, Y., Liu, J., Zhang, H.: Recent advances in real-time spectrum measurement of soliton dynamics by dispersive Fourier transformation. Rep. Prog. Phys. **83**, 116401 (2020)

Wang, T.Y., Zhou, Q., Liu, W.J.: Soliton fusion and fission for the high-order coupled nonlinear Schrödinger system in fiber lasers. Chin. Phys. Lett. **31**, 2 (2022)

Wang, H., Zhou, Q., Liu, W.: Exact analysis and elastic interaction of multi-soliton for a two-dimensional gross-pitaevskii equation in the Bose-Einstein condensation. J. Adv. Res. **38**, 179–190 (2022a)

Wang, H., Li, X., Zhou, Q., Liu, W.: Dynamics and spectral analysis of optical rogue waves for a coupled nonlinear Schrödinger equation applicable to pulse propagation in isotropic media. Chaos, Solitons and Fractals. 166, C (2023)

Xu, N., Ma, P., Fu, S., Shang, X., Jiang, Shouzhen, W., Li, D., Zhang, H.: Tellurene-based saturable absorber to demonstrate large-energy dissipative soliton and noise-like pulse generations. Nanophotonics. **9**, 9 (2020)

Yan, Y.Y., Liu, W.J.: Soliton Rectangular Pulses and bound States in a Dissipative System modeled by the variable-coefficients Complex Cubic-Quintic Ginzburg-Landau equation. Chin. Phys. Lett. **38**, 4 (2022)
Zhao, K., Gao, C., Xiao, X., Yang, C.: Real-time collision dynamics of vector solitons in a fiber laser. Photonics Res. **9**, 289–298 (2021)
Zheng, P., Li, T., Xia, H., Feng, M., Liu, M., Bolin, Y., Luo, A., Xu, W., Luo, Z.: Autosetting soliton pulsation in a fiber laser by an improved depth-first search algorithm. Opt. Express. **29**, 34684–34694 (2021)
Zhou, Y., Ren, Y., Shi, J., Wong, K.: Breathing dissipative soliton explosions in a bidirectional ultrafast fiber laser. Photonics Res. **8**, 1566–1572 (2020a)
Zhou, Y., Ren, Y., Shi, J., Mao, H., Wong, K.: Buildup and dissociation dynamics of dissipative optical soliton molecules. Optica. **7**, 965–972 (2020b)
Zhou, Y., Ren, Y., Shi, J., Wong, K.: Dynamics of breathing dissipative soliton pairs in a bidirectional ultrafast fiber laser. Opt. Lett. **47**, 1968–1971 (2022)

Authors and Affiliations

Yong Zhou[1] · Yangyang Wang[1] · Xian Wang[1] · Kai Zhang[1] · Xiaohui Ma[1] · Wentan Fang[1] · Xiaolin Chen[1] · Wei Zhang[1] · Song Huang[1] · Weiqing Gao[1]

✉ Weiqing Gao
gaoweiqing@hfut.edu.cn

Yong Zhou
yong_zhou@hfut.edu.cn

Yangyang Wang
2020111202@mail.hfut.edu.cn

Xian Wang
2021111185@mail.hfut.edu.cn

Kai Zhang
2021111192@mail.hfut.edu.cn

Xiaohui Ma
mxhui@hfut.edu.cn

Wentan Fang
fwt@hfut.edu.cn

Xiaolin Chen
cxl@hfut.edu.cn

Wei Zhang
weizhang@hfut.edu.cn

Song Huang
huangsong@hfut.edu.cn

[1] School of Physics, Hefei University of Technology, Hefei 230601, China